Hippocampus-Based Static Functional Connectivity Mapping within White Matter in Mild Cognitive Impairment

Yuan Jiang
UESTC: University of Electronic Science and Technology of China
Pan Wang
UESTC: University of Electronic Science and Technology of China https://orcid.org/0000-0003-4074-885X
Jiaping Wen
UESTC: University of Electronic Science and Technology of China
Jianlin Wang
UESTC: University of Electronic Science and Technology of China
Hongyi Li
The Fourth People's Hospital of Chengdu
Bharat B Biswal (bbiswal@gmail.com)
New Jersey Institute of Technology https://orcid.org/0000-0002-3710-3500

Research Article

Keywords: Alzheimer's disease, Functional connectivity, Hippocampus, Mild cognitive impairment, White matter

Posted Date: December 10th, 2021

DOI: https://doi.org/10.21203/rs.3.rs-1106179/v1

Abstract

Mild cognitive impairment (MCI), as the early important stage of Alzheimer's disease (AD), is clinically characterized by memory loss and cognitive impairment closely associated with the hippocampus. Accumulating studies have confirmed the presence of neural signal changes within white matter (WM) in resting-state fMRI. However, how the abnormal hippocampus affects the WM regions remained unclear in MCI. The current study employed 43 MCI, 71 very MCI (VMCI) and 87 matched healthy controls (HC) participants from the public OASIS 3 dataset. Adopting left and right hippocampus (HIP.R) as seed points respectively, whole-brain functional connectivity (FC) maps were obtained for each subject. Subsequently, one-way ANOVA was performed to explore the abnormal FC regions with hippocampus within gray matter (GM)/WM. Further probabilistic tracking was performed to explore whether the abnormal FC corresponded to structural connectivity. Compared to HC, MCI and VMCI groups exhibited common reduced static FC (SFC) in the middle temporal gyrus within GM, and temporal pole and inferior frontal gyrus within WM. Specific dysconnectivity was shown in the cerebellum_crus2 and inferior temporal gyrus within GM, and frontal gyrus within WM. In addition, the fiber bundle connecting the HIP.R and temporal pole within WM showed abnormally increased mean diffusion in MCI. The current study extended a new functional imaging direction for exploring the mechanism of memory decline, and promoted the understanding for pathophysiological mechanism in different early stages of AD.

Introduction

Alzheimer's disease (AD) is a progressive neurodegenerative disease, which has been clinically characterized by memory loss and cognitive impairment, with slow onset and insignificant early symptoms (Rosales-Corral et al. 2012). Very mild cognitive impairment (VMCI) and mild cognitive impairment (MCI) are important transition states between normal aging and AD (Lombardi et al. 2020), in which memory and other cognitive skills decline at a faster rate than expected. However, this decline does not always interfere with a person's ability to perform everyday tasks (Neugroschl and Wang 2011). The annual incidence of MCI to AD was estimated to be about 10–15%, while the basic incidence of AD was 1–2% per year (Lombardi et al. 2020). However, the specific pathogenesis of AD has not been fully elucidated so far. Exploring the abnormality of static functional connectivity (SFC) in white matter (WM) may provide a new method for revealing the neural mechanism of the progressive decline of memory and cognitive function in AD.

The WM accounts for almost half of the human brain, closely connecting to different gray matter (GM) regions (Walhovd et al. 2014). Recent studies have confirmed that the blood-oxygen-level-dependent (BOLD) signal in the WM reflects the neural activity of the human brain (Peer et al. 2017; Wang et al. 2020a; Wang et al. 2021a). Therefore, the fMRI signals from the WM have become a new research direction of fMRI. Several studies on brain diseases have reported abnormal functional connectivity (FC) between different WM and GM regions, such as schizophrenia (Jiang et al. 2019a), epilepsy (Jiang et al. 2019b), Parkinson's Disease (Ji et al. 2019), and pontine strokes (Wang et al. 2019). In addition, Zhao and colleagues demonstrated that the SFC within WM (WM-SFC) of the AD group were significantly lower

than those of the healthy controls (HC) (Zhao et al. 2019). Wang P et al demonstrated the right parahippocampus, posterior cingulate cortex/precuneus, frontal gyrus, and bilateral angular gyrus showed significantly lower connectivity to the left hippocampus (HIP.L) in patients with AD than in HC; the prefrontal cortex, adjunction region of the posterior cingulate cortex and superior occipital cortex, and middle cingulate cortex showed lower connectivity to the right hippocampus (HIP.R) in patients with AD than in HC (Wang et al. 2020b). Wang and colleagues found that compared with HC, participants with MCI and VMCI had significantly lower homotopic FC in the middle occipital gyrus and inferior parietal gyrus of GM (Wang et al. 2021b). They also found decreased homotopic FC in the bilateral middle occipital and parietal lobe in the WM (Wang et al. 2021b). Moreover, Yurui and colleagues found that compared with the cognitively normal group, patients with late MCI and AD dementia had significantly lower FC measurements in the WM, with prominent, specific, and regional defects. (Gao et al. 2020). However, the abnormal connectivity between the hippocampus and WM had not been analyzed in the early stage of AD.

The hippocampus is widely regarded as a critical region of the brain supporting encoding, consolidation and retrieval of memory. It plays a critical role in human memory, implicated in episodic and semantic long-term memory (ILLIAM BEECHER SCOVIILLE 1957; Endel Tulving 1998; Aggleton 2012). Beyond these cognitive functions, the hippocampus is also involved in the regulation of emotion, fear, anxiety, and stress (Bartsch and Wulff 2015). Previous studies have reported the hippocampus to be vulnerable to damage in the early stage of AD (Bradley T. Hyman 2016). At the early stage of MCI, the hippocampus and para hippocampal gyrus shows abnormal atrophy (Jennifer L. Whitwell 2016; Whitwell et al. 2011). By the AD stage, the hippocampus shows a more severe atrophy (Irena S˘te˘pa´n-Buksakowska 2014). In addition, Stepan-Buksakowska and colleagues found that the cortical surface of hippocampus was significantly reduced in the MCI and AD subjects (Irena S˘te˘pa´n-Buksakowska 2014). Functional imaging studies have demonstrated that compared with HC, AD subjects had discernable increases in the low-frequency fluctuations of the hippocampus (Liu et al. 2014). These above studies illuminated that the hippocampus played a vital role in maintaining the normal functional of human brain, and was a core area to understand the specific pathogenesis of AD.

We hypothesized that VMCI and MCI subjects showed abnormal functional and structural connectivity between the bilateral hippocampus and WM regions. To address this hypothesis, we identified and segmented the hippocampus to obtain the hippocampus of each subject. Seed point-based SFC analysis was performed on the whole brain to obtain an SFC diagram of each subject based on the hippocampus. To further explore the differences of hippocampus-based WM-SFC among HC, VMCI, and MCI groups, we performed statistical analysis on SFC maps using one-way ANOVA. The probabilistic tracking was performed to extract the fiber bundles connecting hippocampus and abnormal SFC regions within WM. The averaged mean diffusion (MD) within the fiber bundles was calculated.

Material And Methods

This study used public data from the OASIS-3 dataset (https://central.xnat.org), including 43 MCI, 71 VMCI, and 87 matched HC. Briefly, OASIS-3 is a compilation of MRI and PET imaging data collected from several studies conducted by the Knight AD Research Center at the University of Washington over the past 15 years. The Clinical Dementia Rating (CDR) scale was used to assess the dementia status of uniform data set (UDS) (John C. Morris 2006). According to CDR, all participants were divided into different groups. Specifically, CDR = 0, 0.5 and 1 indicated HC, VMCI and MCI, respectively. Moreover, since the median Mini Mental State Examination (MMSE) could comprehensively and simply reflect the subjects' mental status and degree of cognitive impairment, the MMSE score was collected for each subject (Tom N. Tombaugh 1992). All subjects had provided informed consent before MRI or neurological assessment. In addition, clinical scale information for all patients have been obtained. More detailed information is shown in Table 1.

The MRI images from all the participants were obtained using the 3-T Siemens's Trio Tim scanners. All subjects were instructed to lie quietly and close their eyes during the scan. Resting state functional images were collected using an echo-planner imaging sequence with the following parameters: repetition time (TR) = 2200 ms, echo time (TE) = 27 ms, flip angle (FA) = 90°, number of slices = 33, slice thickness = 4 mm, voxel size = 4×4×4 mm^3. For the T1-weighted images, the parameters are described as follows: voxel size = 1×1×1 mm^3, echo time (TE) = 316 ms, repetition time (TR) = 2400 ms, flip angle = 8°, slice thickness = 1 mm. The echo plane imaging sequence was used to obtain diffusion tensor images (DTI) covering the entire brain, including 24 volumes with diffusion gradients applied along 24 non-collinear directions. The parameters of DTI are as follows: voxel size = 2×2×2 mm^3, echo time = 0.112 s, repetition time = 14.5 s, flip angle = 90°, slice thickness = 2 mm.

Data preprocessing

Resting-state functional images and T1-weighted images preprocessing were performed by using SPM12 (http://www.fil.ion.ucl.ac.uk/spm/software/spm12) and Data Processing Assistant for Resting-State fMRI (http://rfmri.org/DPARSF). Briefly, the functional imaging preprocessing procedures consisted of the following: (1) To remove the unstable signal of the magnetic resonance scanner at the beginning of the scan, the first 5 time points were removed; (2) Head motion correction using rigid body translation and rotation, subjects with maximum motion > 3 mm or 3° were excluded; (3) Anatomical images were co-registered to the mean functional image using a trilinear interpolation with degrees of freedom; (4) For the T1-weighted image data, the DARTEL algorithm was used to segment the GM, WM and cerebrospinal fluid; (5) Regressing interference signal, including 24 head movement parameters and averaging cerebrospinal fluid signal. We did not perform regression on the global signal and the WM signal, to retain as much signals of interest as possible. We used scrubbing when observing movement "spikes" (frame displacement (FD) > 1mm), and performed a separate stopper to reduce movement effects; (6) Removed linear trends to correct signal drift; (7) To minimize the impact of non-neuronal signals on BOLD fluctuations, a band-pass filter of 0.01-0.1 Hz was used to extract the low-frequency components of functional images; (8) To avoid the confusion of WM and GM signals, the WM and GM templates were respectively used to minimize spatial smoothing of the functional images for each subject (4 mm full-

width half-maximum [FWHM], isotropic); (9) The smoothed functional images were normalized from native space to MNI space with voxel size 3Í3Í3 mm³.

DTI were preprocessed and analyzed using FSL (http://www.fmrib.ox.ac.uk/fsl). For each subject, the preprocessing mainly includes removal of non-brain tissue (fractional intensity threshold was 0.2), correction of eddy current distortion, and local fitting of diffusion tensor (Yamada et al. 2014). MD coefficients were calculated based on voxel estimates, and the corresponding files were saved. Then, we performed Bayesian estimation of diffusion parameters obtained using sampling techniques (BEDPOSTX) processing. In this step, BEDPOSTX executes Markov Chain Monte Carlo sampling to establish the distribution of dispersion parameters on each voxel and performs Bayesian estimation at the same time. In order to match the information of the subjects to the same space for comparison, FMRIB's linear image registration tool (FLIRT) was used to run standardization.

The hippocampus masks

To obtain the group-level hippocampus template, we adopted the FMRIB's Integrated Registration and Segmentation Tool on induvidual structural images and obtained the hippocampus mask for each subject (Patenaude et al. 2011). The group-level hippocampus mask was obtained by averaging the individual hippocampus masks across all subjects. Subsequently, a strict threshold of 0.9 was selected to limit above hippocampus mask to obtain the final binarized group-level hippocampus mask. HIP.L and HIP.R were analyzed based on their functional anatomy and potential lateralization (C. Akos Szabo 2001); C Geroldi and colleagues' research based on nuclear magnetic resonance have shown that the bilateral hippocampus of normal adults was a reliable asymmetric structure and dementia was related to the change of normal anatomy asymmetry (C Geroldi 2000).

Creation of group-level WM and GM masks

To avoid mixing the WM and GM signals, we created the group-level WM and GM masks. Specifically, using the WM and GM images segmented from the above T1-weighted structure image, each voxel in the brain was identified with the maximum probability as WM or GM, which created a binary WM and GM mask for each subject. Then, binarized WM masks were averaged and then a threshold with 60% of subjects was used to create a binary group-level WM mask (Jiang et al. 2019a; Peer et al. 2017; Wang et al. 2020a). Adopting the same method, the binarized GM group-level mask was obtained, but using a lenient threshold with 20% of subjects. To further limit the WM and GM group-level masks, we compared the resulting masks to the functional images, and removed voxels identified as WM or GM yet having functional images in less than 80% of the subjects. Finally, to exclude the effect from deep brain structures, we identified the thalamus, caudate, nucleus putamen, globus pallidus and nucleus accumbens based on the Harvard-Oxford template and removed them from the group-level WM mask.

SFC maps with hippocampus as seed point

The current study explored the abnormal SFC between hippocampus and whole-brain voxels in VMCI and MCI subjects. To this end, the following steps were performed: (1) the averaged time series of HIP.L were extracted for each subject; (2) SFC was computed between above time series and all voxels time series within whole brain; (3) Fisher's z transformation was performed for all correlation coefficients. Moreover, we also calculated the SFC between HIP.R and all voxels within whole brain using the above same steps.

Probabilistic tracking analysis

The probabilistic tracking analysis of diffusion tensor imaging (DTI) data was performed using FSL_6.0.3 (https://fsl.fmrib.ox.ac.uk/fsl/fslwiki/). We performed non-invasive probabilistic fiber bundle imaging using probtrackx2. In this step, the distribution estimated by BEDPOSTX was used for simulation. Before the fibers connecting the hippocampus and abnormal WM regions were tracked, these ROIs were transformed from MNI space to individual diffusion space by using FLIRT. Several regions that showed abnormal WM-SFC in patients were selected as regions of interest (ROIs) for analysis of DTI data, and were dilated by two voxels. Finally, FSL repeatedly samples from the main dispersion direction, calculates streamlines through these sampling points, and generates a set of probability streamlines, thereby extracting the fibers between the hippocampus and the abnormal ROI. Through multiple sampling, the prior distribution information was established, and then the true fiber distribution could be inferred from the prior information. The default 0.5 voxel step size, 5000 samples, and 2000 step size were used (–step length 0.5 -P 5000 -S 2000). Finally, we calculated the averaged MD of fiber bundles connecting the hippocampus and ROIs. Two-sample t-test was performed to explore the abnormal structural connectivity between the hippocampus and abnormal WM area between HC, VMCI and MCI ($p < 0.05$/numbers of ROIs, Bonferroni correction was used).

Statistical analysis

Within-group SFC between the HIP.L/HIP.R and voxels within the group-level GM mask was calculated by using one-sample t-test. Abnormal regions of SFC within group-level GM mask among three groups was identified by using one-way ANOVA, with age, gender, and education as covariates. Gaussian Random Field (GRF) theory was performed to correct for cluster-level multiple comparisons (minimum z scores > 2.3; cluster significance: $p < 0.05$, GRF corrected). Three abnormal ROIs were obtained for post-hoc analysis and were compared using the two-sample t-test with age, gender, and education as covariates (two-tailed, $p < 0.05$, Bonferroni-corrected for multiple comparisons ($p < 0.05/3$)).

Moreover, one-sample t-test was calculated for individual SFC maps based on the HIP.L/HIP.R as ROIs across participants in each of the three samples within group-level WM mask. The abnormal regions of SFC within group-level WM mask were obtained among three groups using above similar statistical analysis. Four ROIs were obtained for post-hoc analysis and were compared using the two-sample t-test with age, gender and education as covariates (two-tailed, Bonferroni-corrected for multiple comparisons, $p < 0.05/4$). Finally, Pearson correlation analysis was performed to explore the potential relationships between SFC of abnormal areas and clinical measures.

Results

Clinical data analysis

Demographic information and corresponding clinical information were shown in Table 1, including age, gender, education, handedness and MMSE score. VMCI, MCI and HC have no significant differences in age (one-way ANOVA, $p = 0.7098$), gender (chi-square, $p = 0.2274$), education level (one-way ANOVA, $p = 0.5464$), but one-way ANOVA between the three groups for MMSE scores shows a significant difference with $p < 0.0001$. Moreover, although a few subjects missed the cognitive and memory measures including the logical memory (LOGIMEM), wechsler adult intelligence scale (WAIS), total number of story units recalled (MEMUNITS), and time elapsed since first recall to delayed recall (MEMTIME), we still deal with above information of remain subjects in a comprehensive format to enable readers to have a clearer understanding about the study population (Table 1). One-way ANOVA among three groups showed significant difference with $p < 0.0001$ in the LOGIMEM, WAIS, MEMUNITS, and MEMTIME.

Hippocampus-based SFC within GM

Within-group analysis for hippocampus-based SFC within GM (GM-SFC) showed robust regional differences for each group (Fig 1, (a), (b)). The significance level was set to $p < 0.05$ (uncorrected). In addition, to explore the abnormal SFC among HC, VMCI and MCI, we performed one-way ANOVA for hippocampus-based SFC maps among three groups, and found abnormal SFC between HIP.L and cerebelum_crus2_L (CRcr-II) and cerebelum_7b_R (CR-VIIb), and between HIP.R and inferior temporal gyrus (ITG), cerebelum_crus1_L (CRcr_I), middle temporal gyrus (MTG) and cerebelum_crus2_R (CRcr-II). Subsequently, the post-hoc analysis showed that compared to HC, VMCI and MCI showed abnormal decreased SFC between HIP.R and middle MTG ($p < 0.0001$, $U = 1792$; $p = 0.0002$, $U = 1122$). In addition, MCI showed specifically abnormal decreased SFC between HIP.L and CR-VIIb ($p < 0.0001$, $U = 1055$), and between HIP.R and CRcr-I ($p = 0.0002$, $U = 1140$), CRcr-II ($p = 0.0004$, $U = 1166$), but no difference between VMCI and HC ($p = 0.3409$, $U = 2815$; $p = 0.6034$, $U = 2939$). Finally, compared to HC, MCI showed significant differences between HIP.L and CRcr-II ($p = 0.0005$, $U = 1177$), and between HIP.R and ITG ($p < 0.0001$, $U = 1018$), but no difference between MCI and VMCI ($p = 0.0360$, $U = 1168$; $p = 0.0072$, $U = 1069$), and between VMCI and HC ($p = 0.0914$, $U = 2605$; $p = 0.0150$, $U = 2394$) (Fig 3, (a), (b)).

Hippocampus-based SFC within WM

Since increasing studies reported that the WM BOLD signals could reflect the neuro activities of human brain (Ding et al. 2018; Peer et al. 2017; Jiang et al. 2019a), we further explored the abnormal alterations for SFC between the hippocampus and WM regions. Similar to within-group GM-SFC maps, within-group hippocampus associated WM-SFC maps also showed robust regional differences among the three groups (Fig 2, (a), (b)). Compared to HC, VMCI and MCI showed abnormally decreased SFC between HIP.R and temporal pole-WM (TP-WM) ($p = 0.0002$, $U = 2035$; $p < 0.0001$, $U = 883$), as well as the inferior frontal gyrus-WM (IFG-WM) ($p = 0.0028$, $U = 2238$; < 0.0001, $U = 988$). Moreover, MCI showed abnormal decreased SFC between HIP.L and frontal gyrus within WM (FG-WM) ($p = 0.0003$, $U = 1142$), but no

significant differences between VMCI and HC (p = 0.6757, U = 2968). Finally, compared to HC, MCI showed significant decreased SFC between HIP.R and insula within WM (INS-WM) (p < 0.0001, U = 1094), but no significant difference between MCI and VMCI (p = 0.0320, U =1160), and between VMCI and HC was observed (p = 0.0198, U = 2423) (Fig 4, (a) and (b)).

Probabilistic tracking analysis

Since the structure of the human brain is the foundation of function, structural connectivity was shown to be closely related with the FC in the human brain (Fjell et al. 2017; Huang and Ding 2016). Therefore, we further analyzed the structural connectivity between the hippocampus and regions of abnormal hippocampus-based SFC within WM among HC, VMCI and MCI groups. We found that the abnormal fiber bundles connecting to the HIP.R and TP-WM showed significantly increased MD in MCI subjects compared to HC (p = 0.0074, U = 318). However, no significant differences were found in the TP-WM between HC and VMCI (p = 0.0596, U = 715) (Fig 5).

Relationships between SFC and clinical measures

Pearson correlation analysis was performed to study the potential relationship between SFC of abnormal areas and clinical measures. The average SFC in the MTG with the HIP.R as the ROI was positively correlated with the WAIS score in VMCI group (pi = 0.34, p = 0.01). In addition, the average SFC in the TP-WM based on the HIP.R as the ROI was also positively correlated with the WAIS score in VMCI group (pi = 0.3, p = 0.0292) (Fig 6).

Discussion

The current study explored the hippocampus-based SFC abnormality within WM in the early stage of AD. Within-group analysis showed increased connectivity with $WM\text{-}SFC_{HC} > WM\text{-}SFC_{VMCI} > WM\text{-}SFC_{MCI}$ (Fig. 2), indicating that with the deterioration of the disease, the SFC strength based on hippocampus becomes weaker. We also found abnormal changes of SFC between the bilateral hippocampus and WM regions, as well as the abnormality of structural connectivity within WM, indicating that the memory and cognitive dysfunction of AD were not only related to the GM BOLD signal, but also related to the activities of WM. Our study provided a new fMRI functional direction to explore the pathogenesis and diagnosis of AD.

The hippocampus, as the part of the limbic system in the human brain, is a crucial area responsible for storing and retrieving memories (Callen et al. 2002). For AD patients, the hippocampus was shown to be the first area to be damaged, and also one of the most severely affected areas (Frisoni et al. 2010). The current study found abnormal GM-SFC between the HIP.L and CRcr_II, CR-VIIb, and between HIP.R and ITG, CRcr_I, MTG, and CRcr_II. The cerebellum not only contributes to motor function (A form of familial degeneration of the cerebellum 1908), but also participates in high-level functions related to memory (Schmahmann 2019). Pathological studies demonstrated that the cerebellum largely effected other brain connections (Tang et al. 2021), and is smaller in volume in AD patients (Jacobs et al. 2018). The current

study found the abnormal hippocampus-based SFC in cerebellar regions in the early stages of AD, further elucidating that cerebellar injury might be one of the factors leading to cognitive decline of AD patients. In addition, compared to HC, the volume of the temporal lobe was significantly decreased in the early stages of AD (A. Convit 2000). By examining the correlation between time series of hippocampus and other GM regions, disrupted FC was shown between the HIP.R and temporal lobe in AD (Liang Wang 2005). Temporal lobe facilitates the recovery of spatial position from situational long-term memory (S Köhler 1998; Wheeler 2001), and the damage to temporal lobe leaded to incomplete memory function, which was consistent with abnormal hippocampus-based SFC in the temporal lobe.

Since accumulating studies demonstrated that the BOLD signals within WM could reflect the neuronal actives of human brain (Wang et al. 2021a; Ding et al. 2018), we further explored the abnormal hippocampus-based WM-SFC in the early stages of AD. We found that abnormal SFC based on hippocampus as seed point distributed in the INS-WM, TP-WM, and IFG-WM. In detail, the WM-SFC strength between the HIP.R and TP-WM, IFG-WM in VMCI and MCI was significantly weaker than that of HC (Fig. 4). The connection strength between HIP.L and FG-WM, and between HIP.R and INS of MCI was also weaker than that of HC, indicating that WM lesion was an important factor that affects the cognitive function and memory ability of AD patients. An important function of IFG was to participate in the regulation of attention and cognitive speed (Rektorova 2014). Zhu and colleagues found that compared with HC, the local FC between the bilateral IFG was significantly reduced in AD patients (Zhu et al. 2017). Altered hippocampus-based SFC the INS-WM and IFG-WM may be particularly important in maintaining memory performance in the early stages of AD.

Since the function and structure of human brain were complementary to each other (Sporns 2013), we further explored the structural connectivity between the bilateral hippocampus and abnormal WM-SFC areas. DTI analysis revealed that fiber bundles connecting the HIP.R and TP-WM exhibited an abnormally increased MD in MCI subjects compared to HC (Fig. 5). However, no abnormal structural connectivity between the HIP.R and TP-WM was found between VMCI and HC. Steven E and colleagues found that AD patients showed significant TP atrophy (Steven E. Arnold 1994), which might corresponded to abnormal functional and structural connectivity between HIP.R and TP-WM well. Moreover, the correspondence of functional and structural connectivity between hippocampus and TP-WM further confirmed that the WM BOLD signal could not be simply regarded as noise and could reflect the neural activity of the brain.

In the study, several limitations needed to be clarified. First, The WM BOLD signal was not as strong as the GM BOLD signal, and it was more susceptible to physiological sources such as head movement, respiration, pulsatile blood flow, vasomotor and heart rate changes. Second, the current study did not consider the effects of drugs on results due to a lack of information on medication used. Third, the samples used were cross-sectional, not longitudinal data. Future research is necessary to explore the hippocampus-based WM-SFC changes in the longitudinal dataset of AD. Finally, the DTI data used to explore the structural connectivity between the bilateral hippocampus and ROIs with abnormal functions were not all the resting state data of the subjects, but we have tried our best to collect the DTI data.

Conclusion

In this study, we explored the abnormal changes of hippocampus-based SFC within the whole-brain voxels in the early stage of AD, and further estimated the structural connectivity between the hippocampus and abnormal WM-SFC regions. The TP-WM showed the abnormal functional and structural connectivity to the HIP.R in MCI subjects, indicating that the BOLD signal in WM might be a new direction of the clinical diagnosis of AD.

Declarations

Funding and disclosure

This work was supported by the National Natural Science Foundation of China (grant number: 61871420). The authors declare no conflict of interest.

Data availability statements

Current study employed a public available dataset from the OASIS-3 dataset (https://central.xnat.org). The OASIS-3 is a compilation of MRI and PET imaging data collected from several studies conducted by the Knight AD Research Center at the University of Washington over the past 15 years. All subjects had provided informed consent before MRI or neurological assessment. In addition, clinical scale information for all patients have been obtained.

References

1. A. Convit JdA, M. J. de Leon (2000) Atrophy of the medial occipitotemporal, inferior, and middle temporal gyri in non-demented elderly predict decline to Alzheimer’s disease.
2. Aggleton JP (2012) Multiple anatomical systems embedded within the primate medial temporal lobe: implications for hippocampal function. Neurosci Biobehav Rev 36 (7):1579-1596. doi:10.1016/j.neubiorev.2011.09.005
3. Bartsch T, Wulff P (2015) The hippocampus in aging and disease: From plasticity to vulnerability. Neuroscience 309:1-16. doi:10.1016/j.neuroscience.2015.07.084
4. Bradley T. Hyman GWVH, Antonio R. Damasio and Clifford L. Barnes (2016) Alzheimer's Disease: Cell-Specific Pathology Isolates the Hippocampal Formation.
5. C Geroldi MPL, C DeCarli, A Beltramello, A Bianchetti, H Soininen, M Trabucchi, G B Frisoni (2000) Apolipoprotein E genotype and hippocampal asymmetry in Alzheimer’s disease a volumetric MRI study.
6. C. Akos Szabo JX, Jack L. Lancaster, Lacy Rainey, and Peter Fox (2001) Amygdalar and Hippocampal Volumetry in Control Participants: Differences Regarding Handedness.
7. Callen DJ, Black SE, Caldwell CB (2002) Limbic system perfusion in Alzheimer's disease measured by MRI-coregistered HMPAO SPET. Eur J Nucl Med Mol Imaging 29 (7):899-906.

doi:10.1007/s00259-002-0816-3

8. Ding Z, Huang Y, Bailey SK, Gao Y, Cutting LE, Rogers BP, Newton AT, Gore JC (2018) Detection of synchronous brain activity in white matter tracts at rest and under functional loading. Proc Natl Acad Sci U S A 115 (3):595-600. doi:10.1073/pnas.1711567115
9. Endel Tulving HJM (1998) Episodic and Declarative Memory:Role of the Hippocampus. HIPPOCAMPUS
10. Fjell AM, Sneve MH, Grydeland H, Storsve AB, Amlien IK, Yendiki A, Walhovd KB (2017) Relationship between structural and functional connectivity change across the adult lifespan: A longitudinal investigation. Hum Brain Mapp 38 (1):561-573. doi:10.1002/hbm.23403
11. A form of familial degeneration of the cerebellum (1908).
12. Frisoni GB, Fox NC, Jack CR, Jr., Scheltens P, Thompson PM (2010) The clinical use of structural MRI in Alzheimer disease. Nat Rev Neurol 6 (2):67-77. doi:10.1038/nrneurol.2009.215
13. Gao Y, Sengupta A, Li M, Zu Z, Rogers BP, Anderson AW, Ding Z, Gore JC, Alzheimer's Disease Neuroimaging I (2020) Functional connectivity of white matter as a biomarker of cognitive decline in Alzheimer's disease. PLoS One 15 (10):e0240513. doi:10.1371/journal.pone.0240513
14. Huang H, Ding M (2016) Linking Functional Connectivity and Structural Connectivity Quantitatively: A Comparison of Methods. Brain Connect 6 (2):99-108. doi:10.1089/brain.2015.0382
15. ILLIAM BEECHER SCOVIILLE BM (1957) Loss of recent memory after bilateral hippocampal lesions. J Neurol Neurosurg Psychiat
16. Irena S˘te˘pa´n-Buksakowska M, *w Nikoletta Szabo´, MD,wz Daniel Hor˘ı´nek, MD, PhD (2014) Cortical and Subcortical Atrophy in Alzheimer Disease Parallel Atrophy of Thalamus and Hippocampus. Alzheimer Dis Assoc Disord
17. Jacobs HIL, Hopkins DA, Mayrhofer HC, Bruner E, van Leeuwen FW, Raaijmakers W, Schmahmann JD (2018) The cerebellum in Alzheimer's disease: evaluating its role in cognitive decline. Brain 141 (1):37-47. doi:10.1093/brain/awx194
18. Jennifer L. Whitwell PRCP, MD; Selamawit Negash, PhD; Stephen D. Weigand, MS (2016) Patterns of Atrophy Differ Among Specific Subtypes of Mild Cognitive Impairment.
19. Ji GJ, Ren C, Li Y, Sun J, Liu T, Gao Y, Xue D, Shen L, Cheng W, Zhu C, Tian Y, Hu P, Chen X, Wang K (2019) Regional and network properties of white matter function in Parkinson's disease. Hum Brain Mapp 40 (4):1253-1263. doi:10.1002/hbm.24444
20. Jiang Y, Luo C, Li X, Li Y, Yang H, Li J, Chang X, Li H, Yang H, Wang J, Duan M, Yao D (2019a) White-matter functional networks changes in patients with schizophrenia. Neuroimage 190:172-181. doi:10.1016/j.neuroimage.2018.04.018
21. Jiang Y, Song L, Li X, Zhang Y, Chen Y, Jiang S, Hou C, Yao D, Wang X, Luo C (2019b) Dysfunctional white-matter networks in medicated and unmedicated benign epilepsy with centrotemporal spikes. Hum Brain Mapp 40 (10):3113-3124. doi:10.1002/hbm.24584

22. John C. Morris M, * Sandra Weintraub, PhD,w Helena C. (2006) The Uniform Data Set (UDS): Clinical and Cognitive Variables and Descriptive Data From Alzheimer Disease Centers.
23. Liang Wang YZ, Yong He (2005) Changes in hippocampal connectivity in the early stages of AD. doi:10.1016/j.neuroimage.2005.12.033
24. Liu X, Wang S, Zhang X, Wang Z, Tian X, He Y (2014) Abnormal amplitude of low-frequency fluctuations of intrinsic brain activity in Alzheimer's disease. J Alzheimers Dis 40 (2):387-397. doi:10.3233/JAD-131322
25. Lombardi G, Crescioli G, Cavedo E, Lucenteforte E, Casazza G, Bellatorre AG, Lista C, Costantino G, Frisoni G, Virgili G, Filippini G (2020) Structural magnetic resonance imaging for the early diagnosis of dementia due to Alzheimer's disease in people with mild cognitive impairment. Cochrane Database Syst Rev 3:CD009628. doi:10.1002/14651858.CD009628.pub2
26. Neugroschl J, Wang S (2011) Alzheimer's disease: diagnosis and treatment across the spectrum of disease severity. Mt Sinai J Med 78 (4):596-612. doi:10.1002/msj.20279
27. Patenaude B, Smith SM, Kennedy DN, Jenkinson M (2011) A Bayesian model of shape and appearance for subcortical brain segmentation. Neuroimage 56 (3):907-922. doi:10.1016/j.neuroimage.2011.02.046
28. Peer M, Nitzan M, Bick AS, Levin N, Arzy S (2017) Evidence for Functional Networks within the Human Brain's White Matter. J Neurosci 37 (27):6394-6407. doi:10.1523/JNEUROSCI.3872-16.2017
29. Rektorova I (2014) Resting-state networks in Alzheimer's disease and Parkinson's disease. Neurodegener Dis 13 (2-3):186-188. doi:10.1159/000354237
30. Rosales-Corral SA, Acuna-Castroviejo D, Coto-Montes A, Boga JA, Manchester LC, Fuentes-Broto L, Korkmaz A, Ma S, Tan DX, Reiter RJ (2012) Alzheimer's disease: pathological mechanisms and the beneficial role of melatonin. J Pineal Res 52 (2):167-202. doi:10.1111/j.1600-079X.2011.00937.x
31. S Köhler ARM, M Moscovitch, G Winocur (1998) Functional interactions between the medial temporal lobes and posterior neocortex related to episodic memory retrieval.
32. Schmahmann JD (2019) The cerebellum and cognition. Neurosci Lett 688:62-75. doi:10.1016/j.neulet.2018.07.005
33. Sporns O (2013) Structure and function of complex brain networks. Dialogues in clinical neuroscience 15 (3):247
34. Steven E. Arnold MBTH, MD, PhD; Gary W. Van Hoesen, PhD (1994) Neuropathologic Changes of the Temporal Pole in Alzheimer's Disease and Pick's Disease.
35. Tang F, Zhu D, Ma W, Yao Q, Li Q, Shi J (2021) Differences Changes in Cerebellar Functional Connectivity Between Mild Cognitive Impairment and Alzheimer's Disease: A Seed-Based Approach. Frontiers in Neurology 12:987
36. Tom N. Tombaugh P, CPsych and Nancy J. McIntyre, MA (1992) The Mini-Mental State Examination:
37. A Comprehensive Review.

38. Walhovd KB, Johansen-Berg H, Karadottir RT (2014) Unraveling the secrets of white matter--bridging the gap between cellular, animal and human imaging studies. Neuroscience 276:2-13. doi:10.1016/j.neuroscience.2014.06.058
39. Wang J, Yang Z, Zhang M, Shan Y, Rong D, Ma Q, Liu H, Wu X, Li K, Ding Z, Lu J (2019) Disrupted functional connectivity and activity in the white matter of the sensorimotor system in patients with pontine strokes. J Magn Reson Imaging 49 (2):478-486. doi:10.1002/jmri.26214
40. Wang P, Meng C, Yuan R, Wang J, Yang H, Zhang T, Zaborszky L, Alvarez TL, Liao W, Luo C, Chen H, Biswal BB (2020a) The Organization of the Human Corpus Callosum Estimated by Intrinsic Functional Connectivity with White-Matter Functional Networks. Cereb Cortex 30 (5):3313-3324. doi:10.1093/cercor/bhz311
41. Wang P, Wang J, Tang Q, Alvarez TL, Wang Z, Kung YC, Lin CP, Chen H, Meng C, Biswal BB (2021a) Structural and functional connectivity mapping of the human corpus callosum organization with white-matter functional networks. Neuroimage 227:117642. doi:10.1016/j.neuroimage.2020.117642
42. Wang P, Wang Z, Wang J, Jiang Y, Zhang H, Li H, Biswal BB (2021b) Altered Homotopic Functional Connectivity Within White Matter in the Early Stages of Alzheimer's Disease. Frontiers in Neuroscience:NA
43. Wang P, Zhou B, Yao H, Xie S, Feng F, Zhang Z, Guo Y, An N, Zhou Y, Zhang X, Liu Y (2020b) Aberrant Hippocampal Functional Connectivity Is Associated with Fornix White Matter Integrity in Alzheimer's Disease and Mild Cognitive Impairment. J Alzheimers Dis 75 (4):1153-1168. doi:10.3233/JAD-200066
44. Wheeler RLBaME (2001) THE COGNITIVE NEUROSCIENCE of remembering.
45. Whitwell JL, Jack CR, Jr., Przybelski SA, Parisi JE, Senjem ML, Boeve BF, Knopman DS, Petersen RC, Dickson DW, Josephs KA (2011) Temporoparietal atrophy: a marker of AD pathology independent of clinical diagnosis. Neurobiol Aging 32 (9):1531-1541. doi:10.1016/j.neurobiolaging.2009.10.012
46. Yamada H, Abe O, Shizukuishi T, Kikuta J, Shinozaki T, Dezawa K, Nagano A, Matsuda M, Haradome H, Imamura Y (2014) Efficacy of distortion correction on diffusion imaging: comparison of FSL eddy and eddy_correct using 30 and 60 directions diffusion encoding. PloS one 9 (11):e112411
47. Zhao J, Ding X, Du Y, Wang X, Men G (2019) Functional connectivity between white matter and gray matter based on fMRI for Alzheimer's disease classification. Brain Behav 9 (10):e01407. doi:10.1002/brb3.1407
48. Zhu H, Xu J, Li J, Peng H, Cai T, Li X, Wu S, Cao W, He S (2017) Decreased functional connectivity and disrupted neural network in the prefrontal cortex of affective disorders: A resting-state fNIRS study. J Affect Disord 221:132-144. doi:10.1016/j.jad.2017.06.024

Tables

Table 1. Demographics and clinical characteristics of subjects.

Characteristics	HC (N = 100)	VMCI (N = 90)	MCI (N = 53)	P value
Age	74.29±8.098	74.42±7.749	75.47±9.254	P = 0.7098[a]
Gender (M/F)	45/42	39/32	29/14	P = 0.2274[b]
Education	14.26±1.715	14.69±3.050	14.95±3.177	P = 0.5464[a]
MMSE	28.80±1.328	25.94±2.932	22.16±4.214	P < 0.0001[a]
Handedness (L/R)	0/87	0/71	0/43	
LOGIMEM	12.73±4.240	8.286±4.706	5.025±3.984	P < 0.0001[a]
WAIS	53.51±11.05	40.64±14.25	33.43±15.96	P < 0.0001[a]
MEMUNITS	11.67±4.429	5.886±5.081	3.075±3.805	P < 0.0001[a]
MEMTIME	14.86±2.117	16.66±2.843	17.83±3.802	P < 0.0001[a]
Demographics and clinical characteristics for DTI subjects				
Age	73.38±7.919	76.18±7.451	76.95±7.925	P = 0.1209[a]
Gender (M/F)	26/22	22/17	18/4	P = 0.0719[b]
Education	14.21±1.774	14.90±2.817	15.14±3.028	P = 0.2580[a]
MMSE	29.06±1.137	26.21±2.716	21.64±4.816	P < 0.0001[a]
Handedness (L/R)	0/48	0/39	0/22	

Note: F = female; HC = health control; L = left; LOGIMEM = logical memory; MCI = mild cognitive impairment; M = Male; MMSE = Mini-Mental State Examination; MEMUNITS = total number of story units recalled; MEMTIME = time elapsed since first recall to delayed recall; R = right; VMCI = Very mild cognitive impairment; WAIS = wechsler adult intelligence scale.

[a] One-way ANOVA (using nonparametric test).

[b] Chi-square.

Figures

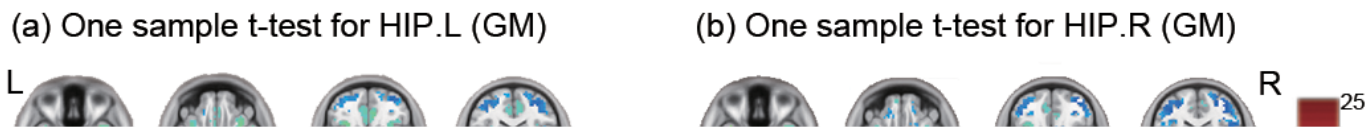

Figure 1

Within-group analysis of hippocampus-based GM-SFC. (a) and (b) respectively represent the SFC maps within GM based on the HIP.L/HIP.R as seed points. Color bar represents the T value. The above brain map is axial. The significant level was set to $p < 0.05$ (uncorrected).

Figure 2

Within-group analysis of hippocampus-based WM-SFC. (a) and (b) respectively represent the SFC maps within WM based on the HIP.L/HIP.R as seed points. Color bar represents the T value. The above brain map is axial. The significant level was set to $p < 0.05$ (uncorrected).

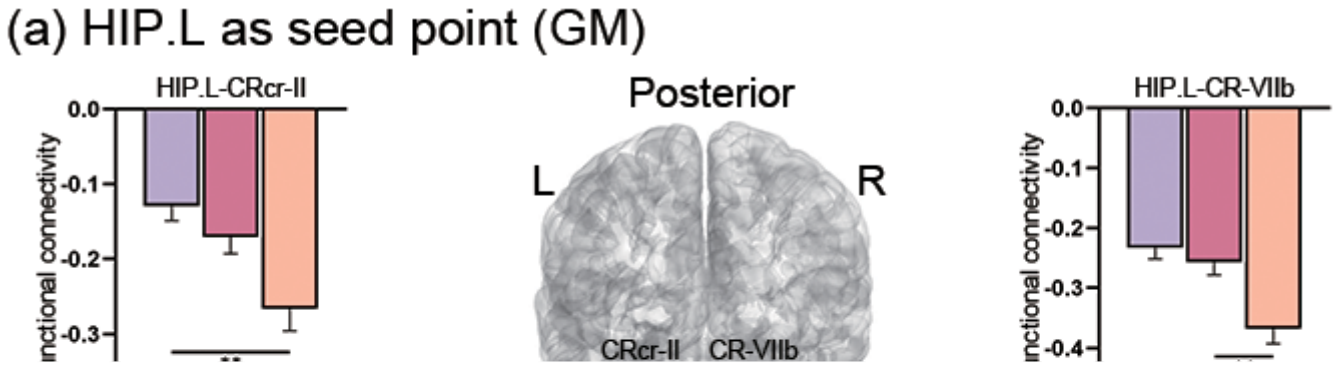

Figure 3

Hippocampus-based GM-SFC. (a) and (b) show the abnormal SFC based on the HIP.L and HIP.R as the seed point within GM, respectively. GRF was used for the cluster-level multiple comparisons correction (minimum z > 2.3; cluster significance: P < 0.05, GRF corrected). In addition, ** represents the p < 0.05/numbers of ROIs, Bonferroni correction.

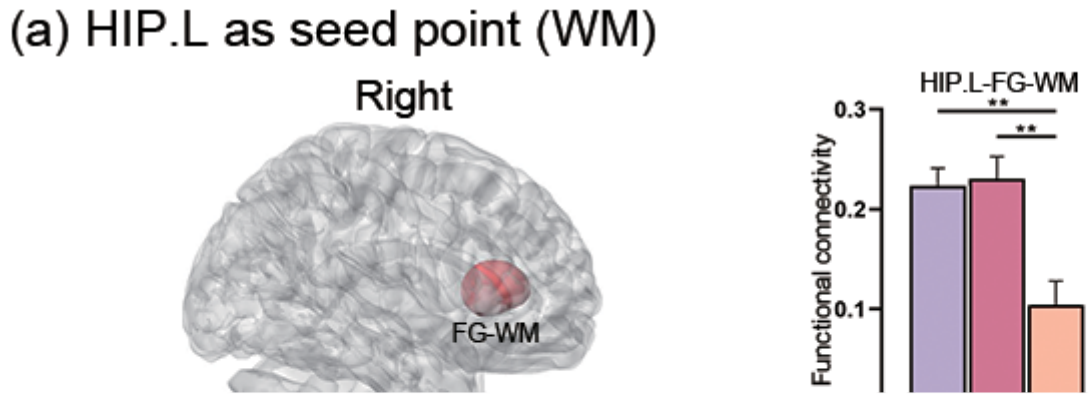

Figure 4

Hippocampus-based WM-SFC. (a) and (b) show the abnormal SFC based on the HIP.L and HIP.R as the seed point within WM, respectively. GRF was used for the cluster-level multiple comparisons correction (minimum z > 2.3; cluster significance: P < 0.05, GRF corrected). In addition, ** represents the p < 0.05/numbers of ROIs, Bonferroni correction.

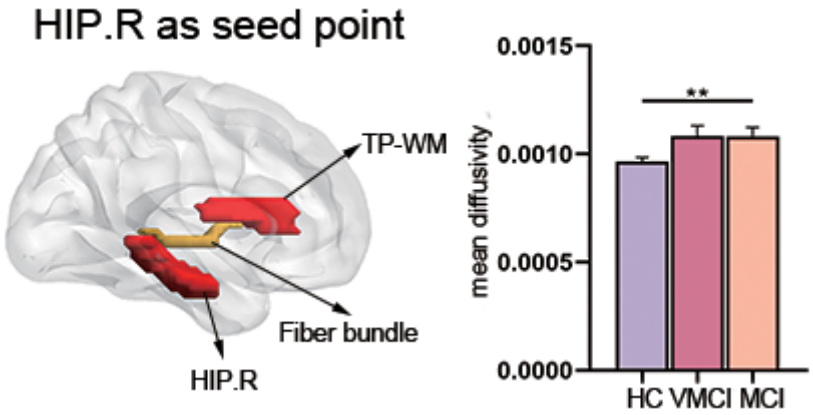

Figure 5

Altered structural connectivity between HIP.R and TP-WM. Left portion represents the brain map showing the fiber bundle connecting the HIP.R and TP-WM. Right portion represents the bar charts showing the abnormal MD in MCI subjects compared to HC. ** represents the $p < 0.05$/numbers of ROIs, Bonferroni correction.

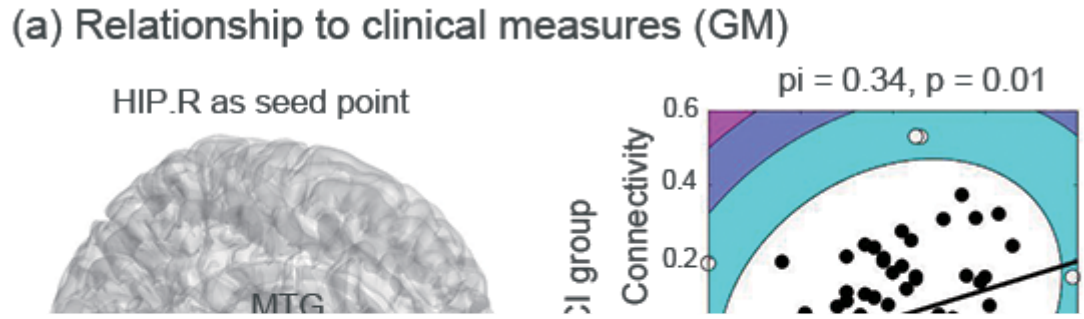

Figure 6

Correlations between SFC and clinical measures. (a) The mean SFC within MTG was positively correlated with WAIS score in VMCI group (pi = 0.34, p = 0.01). (b) The mean SFC within TP-WM was positively correlated with WAIS score in VMCI group (pi = 0.3, p = 0.0292).